

More on a possible energy dependence of Θ_{13} in vacuum neutrino oscillations

Frans R. Klinkhamer*

*Institute for Theoretical Physics,
University of Karlsruhe (TH),
76128 Karlsruhe, Germany*

Abstract

Vacuum neutrino-oscillation probabilities from a simple three-flavor model with both mass-square differences and timelike Fermi-point splittings have been presented in a previous article [hep-ph/0504274]. Here, further results are given: first, for specific parameters relevant to MINOS in the low-energy mode and, then, for arbitrary parameters. A generalized model with equidistant Fermi-point splittings and an additional complex phase is also discussed. If relevant, this generalized model might have interesting effects at future long-baseline oscillation experiments.

PACS numbers: 14.60.St, 11.30.Cp, 73.43.Nq

Keywords: Non-standard-model neutrinos, Lorentz noninvariance, Quantum phase transition

*Electronic address: frans.klinkhamer@physik.uni-karlsruhe.de

I. INTRODUCTION

In a previous article [1], we have considered a simple three-flavor neutrino-oscillation model with both mass-square differences (Δm_{ij}^2) and timelike Fermi-point splittings ($\Delta b_0^{(ij)}$). The mixing of the mass sector is taken to be bi-maximal and the one of the Fermi-point-splitting sector trimaximal, with all complex phases vanishing. The model has furthermore a hierarchy of Fermi-point splittings ($b_0^{(1)} = b_0^{(2)} \neq b_0^{(3)}$) which parallels the hierarchy of masses ($m_1 = m_2 \neq m_3$). This particular model may be called the “stealth model,” as it allows for Lorentz-noninvariant Fermi-point-splitting effects to hide behind mass-difference effects. For the physics motivation of this type of model discussion, see Ref. [1] and references therein.

The present article follows up the previous one in three ways. First, we give model results of the vacuum appearance probability $P(\nu_\mu \rightarrow \nu_e)$ relevant to MINOS in the low-energy mode, complementing the specific results for the medium energy mode in Ref. [1].

Second, we consider the model probability $P_{\mu e} \equiv P(\nu_\mu \rightarrow \nu_e)$ for the case of relatively strong Fermi-point-splitting effects compared to mass-difference effects, whereas Ref. [1] focused on relatively weak splitting effects. In particular, we introduce a new parametrization (with nonnegative dimensionless parameters ρ and τ) which makes a straightforward comparison between different long-baseline neutrino-oscillation experiments possible. Relatively weak or strong Fermi-point-splitting effects then correspond to $\rho\tau \ll 1$ or $\rho\tau \gtrsim 1$, respectively. The behavior of $P_{\mu e}(\rho, \tau)$ turns out to be quite complicated for $\rho\tau \gtrsim 1$,

Third, we present results on the appearance probability $P(\nu_\mu \rightarrow \nu_e)$ from a generalized model with the same mass hierarchy as the model of Ref. [1] but with equidistant Fermi-point splittings ($b_0^{(2)} - b_0^{(1)} = b_0^{(3)} - b_0^{(2)}$) and one additional complex phase ($\omega = \pi/4$). For completeness, we also give the model probability of the time-reversed process, $\nu_e \rightarrow \nu_\mu$. It will be seen that the generalized model has a rather interesting phenomenology with stealth-like characteristics in certain cases and strong time-reversal noninvariance in others.

The outline for the remainder of this article is as follows. In Sec. II, we recall the definition of the model and introduce the two neutrino-oscillation parameters ρ and τ . In Sec. III, we present and discuss our new results. In the Appendix, we consider one concrete model and compare the capabilities of four accelerator-based long-baseline oscillation experiments.

II. MODEL

Setting $\hbar = c = 1$ and writing $p \equiv |\vec{p}|$ for the neutrino momentum, the Hamiltonian of the stealth model [1] contains three terms in the $(\nu_e, \nu_\mu, \nu_\tau)$ flavor basis,

$$H \supset p \mathbb{1} + X \cdot D_m \cdot X^{-1} + Y \cdot D_{b_0} \cdot Y^{-1}, \quad (1)$$

with diagonal matrices

$$D_m \equiv \text{diag} \left(\frac{m_1^2}{2p}, \frac{m_2^2}{2p}, \frac{m_3^2}{2p} \right), \quad D_{b_0} \equiv \text{diag} \left(b_0^{(1)}, b_0^{(2)}, b_0^{(3)} \right), \quad (2)$$

and $SU(3)$ matrices

$$X \equiv M_{32}(\theta_{32}) \cdot M_{13}(\theta_{13}, \delta) \cdot M_{21}(\theta_{21}), \quad Y \equiv M_{32}(\chi_{32}) \cdot M_{13}(\chi_{13}, \omega) \cdot M_{21}(\chi_{21}), \quad (3)$$

in terms of the basic matrices

$$M_{32}(\vartheta) \equiv \begin{pmatrix} 1 & 0 & 0 \\ 0 & \cos \vartheta & \sin \vartheta \\ 0 & -\sin \vartheta & \cos \vartheta \end{pmatrix}, \quad M_{21}(\vartheta) \equiv \begin{pmatrix} \cos \vartheta & \sin \vartheta & 0 \\ -\sin \vartheta & \cos \vartheta & 0 \\ 0 & 0 & 1 \end{pmatrix},$$

$$M_{13}(\vartheta, \varphi) \equiv \begin{pmatrix} \cos \vartheta & 0 & +e^{+i\varphi} \sin \vartheta \\ 0 & 1 & 0 \\ -e^{-i\varphi} \sin \vartheta & 0 & \cos \vartheta \end{pmatrix}, \quad (4)$$

and the following parameters:

$$\Delta m_{21}^2 \equiv m_2^2 - m_1^2 = 0, \quad R \equiv \Delta b_0^{(21)} / \Delta b_0^{(32)} \equiv (b_0^{(2)} - b_0^{(1)}) / (b_0^{(3)} - b_0^{(2)}) = 0, \quad (5a)$$

$$\theta_{13} = 0, \quad \theta_{21} = \theta_{32} = \chi_{13} = \chi_{21} = \chi_{32} = \pi/4, \quad (5b)$$

$$\delta = \omega = 0. \quad (5c)$$

With all other complex phases vanishing, there are only two neutrino-oscillation parameters left in the model,

$$\Delta m_{31}^2 \equiv m_3^2 - m_1^2 > 0, \quad \Delta b_0^{(31)} \equiv b_0^{(3)} - b_0^{(1)} > 0, \quad (6)$$

which have been taken positive.

For high-energy neutrino oscillations over a travel distance L , there are, then, two dimensionless parameters which completely define the problem, at least for the simple model considered and matter effects neglected. These neutrino-oscillation parameters can be defined as follows ($E_\nu \sim p$):

$$\rho \equiv \frac{2 E_\nu \hbar c}{|\Delta m_{31}^2| c^4 L} \approx \left(\frac{2.5 \times 10^{-3} \text{ eV}^2 / c^4}{|\Delta m_{31}^2|} \right) \left(\frac{735 \text{ km}}{L} \right) \left(\frac{E_\nu}{4.656 \text{ GeV}} \right), \quad (7a)$$

$$\tau \equiv \frac{L |\Delta b_0^{(31)}|}{\hbar c} \approx \left(\frac{|\Delta b_0^{(31)}|}{2.685 \times 10^{-13} \text{ eV}} \right) \left(\frac{L}{735 \text{ km}} \right), \quad (7b)$$

with \hbar and c temporarily reinstated.

In terms of these parameters, an approximate formula for the vacuum probability $P_{\mu e} \equiv P(\nu_\mu \rightarrow \nu_e)$ is given by [1]

$$P_{\mu e}^{\text{stealth}}(\rho, \tau) \sim (1/2) \sin^2(2\Theta_{13}) \sin^2 \left(\left[\rho^{-1} + \tau + \sqrt{\rho^{-2} + \tau^2} \right] / 4 \right), \quad (8a)$$

with the following energy-dependent effective mixing angle:

$$\Theta_{13}(\rho, \tau) \sim (1/2) \arctan(\rho \tau). \quad (8b)$$

Recall that, according to Eq. (5b), the bare mixing angle θ_{13} vanishes identically and that, as mentioned above, matter effects are neglected in this approximate model probability [2].

More generally and allowing for a nonzero Fermi-point-splitting ratio R , one can define

$$P_{\mu e}^{\text{stealth}}(\rho, \tau) = \sin^2(\widehat{\Theta}_{32}) \sin^2(2\widehat{\Theta}_{13}) \widehat{\Lambda}_{\mu e}^2, \quad (9a)$$

with the following functional dependence:

$$\widehat{\Theta}_{32} = \widehat{\Theta}_{32}(\rho\tau, R), \quad \widehat{\Theta}_{13} = \widehat{\Theta}_{13}(\rho\tau, R), \quad \widehat{\Lambda}_{\mu e} = \widehat{\Lambda}_{\mu e}(\rho, \tau, R) \in [-1, +1], \quad (9b)$$

so that the effective mixing angles $\widehat{\Theta}_{32}$ and $\widehat{\Theta}_{13}$ are independent of the travel distance L , according to Eqs. (7ab), whereas $\widehat{\Lambda}_{\mu e}$ does depend on L [5]. In principle, $\widehat{\Theta}_{13}$ does not have to vanish in the limit $\rho \rightarrow 0$ for fixed τ and this is indeed the case for the generalized model with splitting ratio $R \neq 0$ (see below).

III. RESULTS AND DISCUSSION

In Ref. [1], we have given five figures with model results, three of which may be relevant to T2K or NO ν A and two to MINOS in the medium-energy (ME) mode. Here, we present one more figure, Fig. 1, which may be relevant to MINOS (baseline $L = 735$ km) in the *low-energy* (LE) mode, with peak neutrino energy \overline{E}_ν approximately equal to 3.75 GeV and neutrino-oscillation length scale $\overline{L} \equiv 2\pi\overline{E}_\nu/|\Delta m_{31}^2| \approx 1860$ km for $\Delta m_{31}^2 = 2.5 \times 10^{-3}$ eV². Figure 1 (which may be compared to Figs. 4 and 5 of Ref. [1]) shows that, if MINOS–LE would be able to place an upper limit of 10% on the appearance probability $P(\nu_\mu \rightarrow \nu_e)$ at the high end of the energy spectrum ($E_\nu \gtrsim 4$ GeV), this would correspond to an upper limit on $|\Delta b_0^{(31)}|$ of approximately 3×10^{-13} eV (assuming $\tau \leq \pi$, see below).

A further figure, Fig. 2, gives numerical results which illustrate the general behavior of the vacuum probability $P_{\mu e} \equiv P(\nu_\mu \rightarrow \nu_e)$ as a function of the two dimensionless parameters ρ and τ from Eqs. (7ab). Note that we expect $\lim_{\tau \rightarrow 0} P_{\mu e}(\rho, \tau)$ to vanish [pure mass-difference model with $\Delta m_{21}^2 = 0$ and $\theta_{13} = 0$] and $\lim_{\rho \rightarrow \infty} P_{\mu e}(\rho, \tau)$ to be given by $(1/2) \sin^2(\tau/2)$ [pure Fermi-point-splitting model with $\Delta b_0^{(21)} = 0$, $\Delta b_0^{(31)} \neq 0$, and trimaximal mixing]. The landscape of Fig. 2 can then be described as follows: mountain ridges start out at $\rho \gg 1$ and $\tau \approx n_\infty \pi$ for odd integers n_∞ , slope down towards lower values of ρ keeping approximately the same values of τ , and, finally, disappear while bending towards lower values of τ (more so for ridges with large n_∞). This topography is qualitatively reproduced by the analytic expression (8).

Figure 3 presents a sequence of constant- τ slices of the vacuum probability $P_{\mu e}(\rho, \tau)$ from Fig. 2. The behavior of $P_{\mu e}(\rho, \tau)$ at $\tau = 2\pi$ (or integer multiples thereof) is quite remarkable, being nonzero only for a relatively small range of energies; cf. the short-dashed curve in the upper right panel of Fig. 3.

Next, turn to a generalized stealth model with splitting ratio $R = 1$ (i.e., equidistant Fermi-point splittings) and complex phase $\omega = 0$ or $\pi/4$, the other model parameters being

kept at the values (5abc) and maintaining the signs (6). (For high energies, this model is similar to the pure Fermi-point-splitting model studied previously [6, 7].) Figures 4 and 5 give the resulting vacuum probabilities $P_{\mu e} \equiv P(\nu_\mu \rightarrow \nu_e)$ [8, 9]. For both complex phases, the behavior of $P_{\mu e}(\rho, \tau)$ at $\tau \approx 12$ is particularly noteworthy; cf. the short-dashed curves in the lower right panels of Figs. 4 and 5. At the corresponding distance L for given value of the Fermi-point splitting $\Delta b_0^{(31)}$, namely, the stealth model lives up to its name by evading detection via ν_e appearance, unless the experiment is able to reach down to low enough neutrino energies ($\rho \sim 0.15$). In principle, the way to corner this stealth model would be to use several broad-band experiments at *different* baselines, but this may require a substantial effort (see the Appendix for a case study).

In the previous paragraph and corresponding Appendix, the stealth-like behavior of the $R = 1$, $\omega = \pi/4$ model has been emphasized, but this holds only for the $\nu_\mu \rightarrow \nu_e$ channel relevant to superbeam experiments with an initial ν_μ beam from pion and kaon decays. In other channels, the situation may be different. The probability $P_{e\mu}$ of the $\nu_e \rightarrow \nu_\mu$ channel, for example, is given in Fig. 6. The very different probabilities of Figs. 5 and 6, for $\rho \gtrsim 0.2$ and generic values of τ , signal time-reversal (T) noninvariance.

For comparison, we give in Figs. 7–10 the numerical results from a “realistic” mass sector: $R_m \equiv \Delta m_{21}^2 / \Delta m_{32}^2 \approx 0.033$, $\sin^2(2\theta_{13}) = 0.1$ [close to the experimental bound from Chooz], and two possible values of the complex phase, $\delta = 0$ or $\delta = \pi/2$. Figures 9 and 10, in particular, show that the maximum T-violation discriminant $\Delta_T \equiv P_{e\mu} - P_{\mu e}$ from pure mass-difference neutrino oscillations ($\tau = 0$) is of the order of several percent, much less than the potential Fermi-point-splitting result (several tens of percent) at the high-energy end of the neutrino spectrum.

The strong high-energy T violation (and possibly CP violation [7]) from Figs. 5–10 traces back to the large complex phase ω of the model considered, together with the large mixing angles χ_{ij} and splitting ratio R in the Fermi-point-splitting sector. In other words, the breaking of time-reversal invariance would primarily take place outside the mass sector. A neutrino factory (see Ref. [3] and the Appendix) would be the ideal machine, in principle, to establish such strong T violation in high-energy neutrino oscillations.

ACKNOWLEDGMENTS

It is a pleasure to thank Jacob Schneps for useful discussions and Elisabeth Kant and Christian Kaufhold for help with the references and the figures.

APPENDIX A: CASE STUDY

In this appendix, we give a concrete example of the complicated phenomenology of stealth-type models. Take, then, the generalized model (1)–(6) with parameters $\omega = \pi/4$

and $\Delta b_0^{(31)} = 2\Delta b_0^{(21)} = 3.5 \times 10^{-12}$ eV and consider the *combined* performance of four accelerator-based neutrino-oscillation experiments [10, 11]: the current K2K experiment (baseline $L = 250$ km and peak energy $\overline{E}_\nu \approx 1.0$ GeV), the running MINOS experiment ($L = 735$ km and $\overline{E}_\nu \approx 3.75$ GeV, in the LE mode), the planned T2K experiment ($L = 295$ km and $\overline{E}_\nu \approx 0.7$ GeV, for an off-axis beam at 2 degrees), and the proposed NO ν A experiment ($L = 810$ km and $\overline{E}_\nu \approx 2$ GeV, at 14 mrad offset in the ME mode). At the end of this appendix, we also comment briefly on the capabilities of a possible neutrino factory.

First, calculate the model predictions for the two current experiments. For K2K, the neutrino-oscillation parameters would be $\tau \approx 4.4$ and $\rho \approx 0.63$, so that a value for $P_{\mu e} \equiv P(\nu_\mu \rightarrow \nu_e)$ of only 1% would be expected (cf. solid curve in upper right panel of Fig. 5), which is consistent with the experimental result [13]. [Note that the K2K appearance probability $P_{\mu e}$ would be approximately 15% for the model with vanishing complex phase ω , as indicated by the solid curve in the upper right panel of Fig. 4.] For the MINOS–LE experiment with $\tau \approx 13.0$ and $\rho \approx 0.81$, a relatively small probability $P_{\mu e} \approx 7\%$ would be expected, which would perhaps be hard to separate from the background. [Note that this τ -value corresponding to the MINOS baseline is an order of magnitude above the largest one of Fig. 1.] Hence, the model predictions of the appearance probability $P_{\mu e}$, for the chosen parameters, would be consistent with rather low ν_e event rates from both of these current experiments. For completeness, the model would also give a survival probability $P_{\mu\mu} \equiv P(\nu_\mu \rightarrow \nu_\mu)$ of some 49% for K2K and 87% for MINOS–LE.

Next, turn to the model predictions for the two future experiments considered. For T2K with $\tau \approx 5.2$ and $\rho \approx 0.38$, a substantial $P_{\mu e}$ of some 25% would be expected (cf. long-dashed curve in upper right panel of Fig. 5). Similarly, for NO ν A with $\tau \approx 14.4$ and $\rho \approx 0.39$, $P_{\mu e}$ would be approximately 27%. Hence, the model predictions of the appearance probability $P_{\mu e}$ would imply a clear signal in these future experiments, at least for the chosen parameters. Again, for completeness, the model survival probability $P_{\mu\mu}$ would be approximately 71% for T2K and 20% for NO ν A.

Ultimately, the lowest values of $|\Delta b_0^{(31)}|$ could be probed by a neutrino factory with broad energy spectrum $E_\nu \approx 10 - 50$ GeV and several detectors at baselines L up to 12800 km; see, e.g., Refs. [3, 4, 12]. For a quick estimate, one can simply compare the expected experimental capabilities with the approximate vacuum probability (8), for $\rho = O(1)$ and $\tau \ll 1$ as defined by (7). In the best of all worlds, a $P_{\mu e}$ sensitivity of 0.01% at $L = 7350$ km and $E_\nu \approx 46$ GeV, for example, would correspond to $|\Delta b_0^{(31)}|$ of the order of 10^{-15} eV. However, for a definite analysis at these large distances, matter effects [2] would need to be folded in.

[1] F.R. Klinkhamer, “Possible energy dependence of Θ_{13} in neutrino oscillations,” Phys. Rev. D **71**, 113008 (2005) [hep-ph/0504274].

- [2] Matter effects (coherent forward scattering) from the Earth’s mantle become important for standard mass-difference neutrino oscillations at energies E_ν of order 10 GeV and travel distances L of order 2500 km. For further details and references, see, e.g., Ref. [3] and Ref. [4], Chapter 3 [hep-ph/0210192].
- [3] A. Bueno, M. Campanelli, S. Navas-Concha, and A. Rubbia, “On the energy and baseline optimization to study effects related to the δ -phase (CP-/T-violation) in neutrino oscillations at a neutrino factory,” Nucl. Phys. B **631**, 239 (2002) [hep-ph/0112297].
- [4] A. Blondel *et al.*, *ECFA/CERN studies of a European neutrino factory complex*, report CERN-2004-002, April 2004.
- [5] In the combined limit $\rho \rightarrow \infty$ and $\tau \rightarrow 0$, the factor $\widehat{\Lambda}_{\mu e}$ behaves as $O(1/\rho) + O(\tau)$, i.e., proportional to L . Note also that, in first approximation, $\widehat{\Lambda}_{\mu e}$ is assumed to contain no further factors which only depend on the product $\rho\tau$. In addition, it is necessary to consider all channels in order to make, as far as possible, a useful distinction between the quantities $\widehat{\Theta}_{32}$ and $\widehat{\Theta}_{13}$ in Eq. (9a).
- [6] F.R. Klinkhamer, *Neutrino oscillations from the splitting of Fermi points*, JETP Lett. **79**, 451 (2004) [hep-ph/0403285].
- [7] F.R. Klinkhamer, *Lorentz-noninvariant neutrino oscillations: Model and predictions*, Int. J. Mod. Phys. A **21**, 161 (2006) [hep-ph/0407200].
- [8] Note that the notation for the neutrino dispersion relation in Refs. [6, 7] differs from the one used here and in Ref. [1]. For neutrino oscillations in the pure Fermi-point-splitting model [6, 7], the different sign of $b_0^{(f)}$ can be compensated by a sign change of the complex phase ϵ . For example, setting $\epsilon = -\omega$ in the exact model probability $P_{\mu e}$ from Eq. (11e) of Ref. [7] reproduces the numerical $\rho \rightarrow \infty$ results for $R = 1$, $\chi_{21} = \chi_{32} = \pi/4$, $\chi_{13} = \arctan \sqrt{1/2} \approx \pi/5$, and $\omega = 0$ or $\pi/4$ (these numerical results closely resemble those for $\chi_{13} = \pi/4$ presented in Figs. 4 and 5 here).
- [9] Degenerate perturbation theory for $\rho \rightarrow 0$ and fixed τ (arbitrary R and ω) gives $P_{\mu e} \sim (4R^2/S) \sin^2[\sqrt{S}\tau/(8 + 8R)]$ with $S \equiv 4 + 4R + 9R^2$. For $R = 1$, in particular, the $\rho \rightarrow 0$ probability is given by $P_{\mu e} \sim (4/17) \sin^2[\sqrt{17}\tau/16]$. If, however, the mass-hierarchy parameter $R_m \equiv \Delta m_{21}^2/\Delta m_{32}^2$ is changed from zero to $1/30$, the $\rho \lesssim 0.1$ behavior changes significantly, as will become clear later on.
- [10] S. T’Jampens, *Current and near future long-baseline neutrino experiments*, in Ref. [12], p. 24.
- [11] D.A. Harris, *Superbeam Experiments*, in Ref. [12], p. 34.
- [12] *Proceedings 6th International Workshop on Neutrino Factories and Superbeams (NuFact04)*, edited by M. Aoki, Y. Iwashita, and M. Kuze, Nucl. Phys. B (Proc. Suppl.) **149** (2005), pp. 1–411.
- [13] M.H. Ahn *et al.* [K2K Collaboration], *Search for electron neutrino appearance in a 250-km long-baseline experiment*, Phys. Rev. Lett. **93**, 051801 (2004), hep-ex/0402017; K. Kaneyuki, *K2K far detector analysis*, in Ref. [12], p. 119.

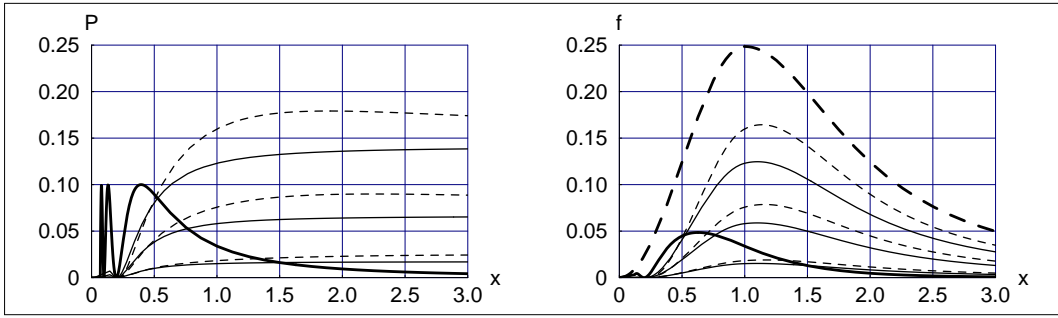


FIG. 1: Left: Fixed-distance vacuum probabilities $P_{\mu e} \equiv P(\nu_\mu \rightarrow \nu_e)$ at $l \equiv L/\bar{L} \equiv L|\Delta m_{31}^2|/(2\pi\bar{E}_\nu) = 735/1860$ vs. dimensionless energy $x \equiv E_\nu/\bar{E}_\nu$ for the “stealth” model of Ref. [1] with both mass differences and timelike Fermi-point splittings, here defined by Eqs. (1)–(6). The broken curves are given by the analytic expression (4.4) of Ref. [1] with parameters $\bar{\Theta}_{13} \equiv \bar{E}_\nu |\Delta b_0^{(31)}|/|\Delta m_{31}^2| = 0.15, 0.30, 0.45$, which correspond to Fermi-point splittings $|\Delta b_0^{(13)}| \approx (1.0, 2.0, 3.0) \times 10^{-13}$ eV for $\bar{E}_\nu = 3.75$ GeV and $\Delta m_{31}^2 = 2.5 \times 10^{-3}$ eV². The same analytic expression is given here by Eq. (8) with parameters $\tau \approx (0.37, 0.74, 1.12)$. These broken curves are only approximate and the corresponding thin solid curves give the full numerical results. The heavy solid curve gives, for comparison, the standard mass-difference probability $P_{\mu e}^{\text{MD}}$ for $\Delta m_{21}^2 = 0$, $\sin^2 \theta_{32} = 1/2$, $\sin^2(2\theta_{13}) = 0.2$, and $l = 735/1860$. Right: Electron-type neutrino energy spectra $f_e(x)$ at $l = 735/1860$ from an initial muon-type spectrum (4.8) of Ref. [1] at $l = 0$ and vacuum probabilities $P(\nu_\mu \rightarrow \nu_e)$ of the left panel. The initial ν_μ spectrum multiplied by a constant factor 0.25 is shown as the heavy long-dashed curve. The resulting ν_e spectra from the “stealth” model are shown as the thin solid curves [approximate values as thin broken curves]. The heavy solid curve gives, for comparison, the ν_e spectrum from the standard mass-difference probability $P_{\mu e}^{\text{MD}}$ of the left panel.

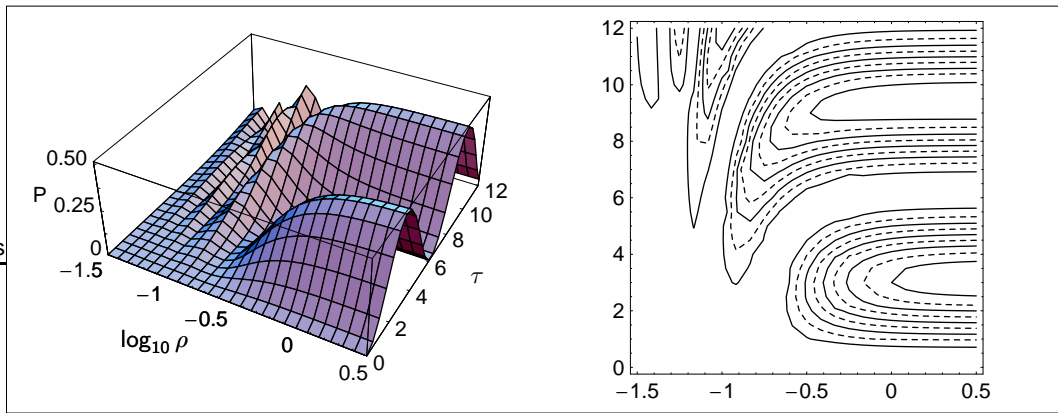


FIG. 2: Numerical results for the vacuum probability $P_{\mu e} \equiv P(\nu_\mu \rightarrow \nu_e)$ from the “stealth” model (1)–(6), as a function of the two dimensionless parameters ρ and τ , defined by Eqs. (7ab). Left: surface plot. Right: contour plot, with equidistant contours at $P_{\mu e} = 0.05, 0.10, 0.15, \dots, 0.45$ and contours at integer multiples of 0.10 shown dashed.

$R = 0, \omega = 0$

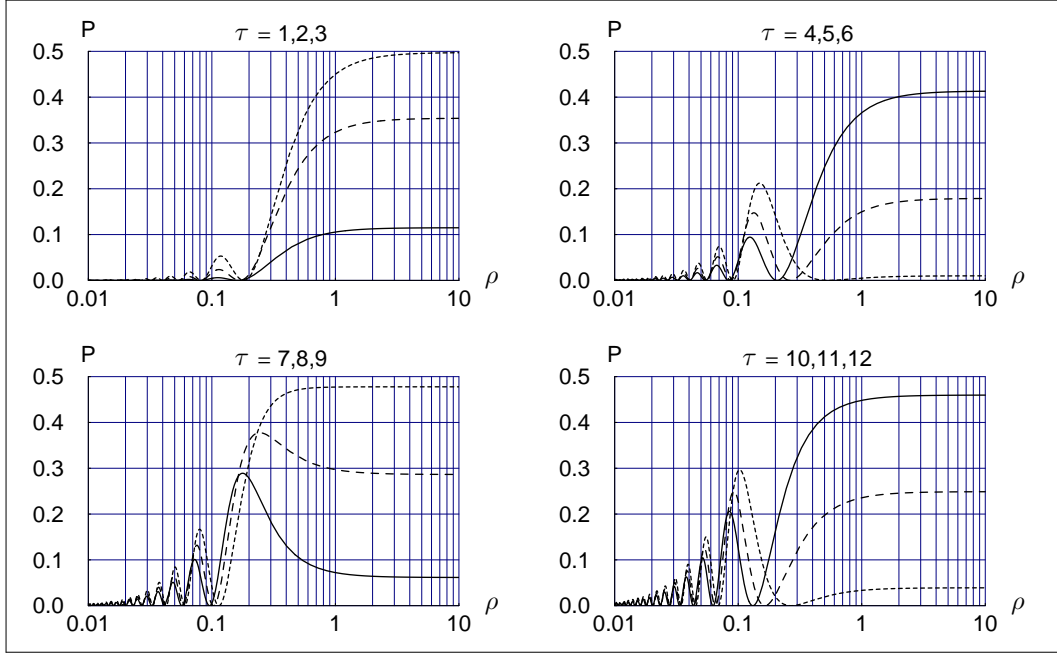


FIG. 3: Numerical results for constant- τ slices of the vacuum probability $P \equiv P(\nu_\mu \rightarrow \nu_e)$ from Fig. 2. The curves for positive $\tau = 1, 2, 0 \pmod{3}$ are shown as solid, long-dashed, and short-dashed lines, respectively. For the simple model considered, given by Eqs. (1)–(6), the parameters R and ω vanish identically.

$R = 1, \omega = 0$

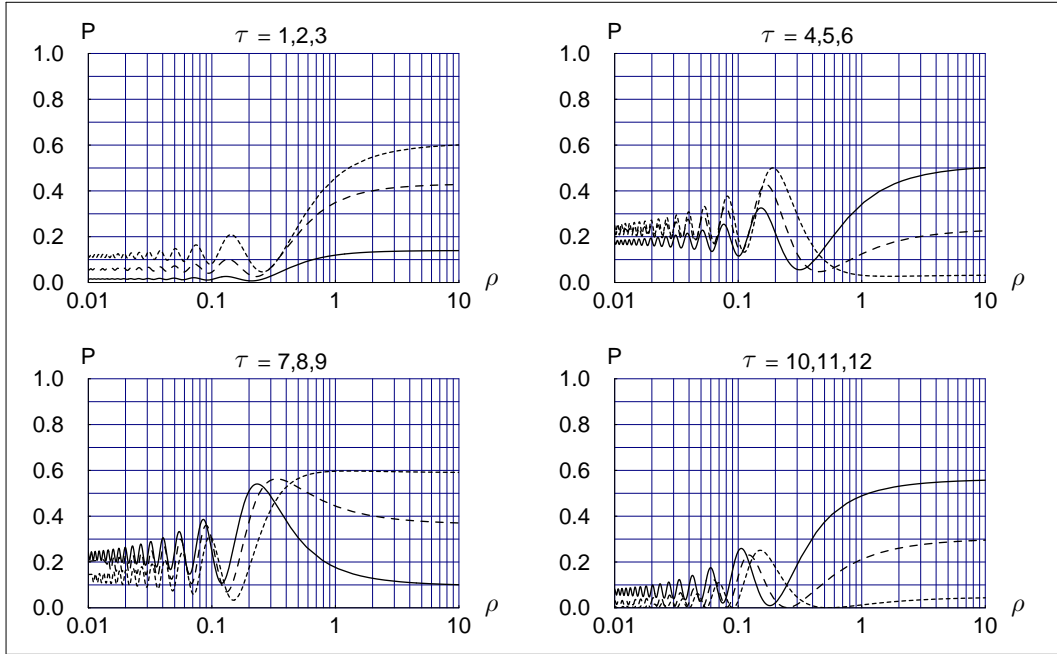


FIG. 4: Same as Fig. 3 but for the generalized model with splitting ratio $R \equiv |\Delta b_0^{(21)} / \Delta b_0^{(32)}| = 1$, the complex phase ω still vanishing.

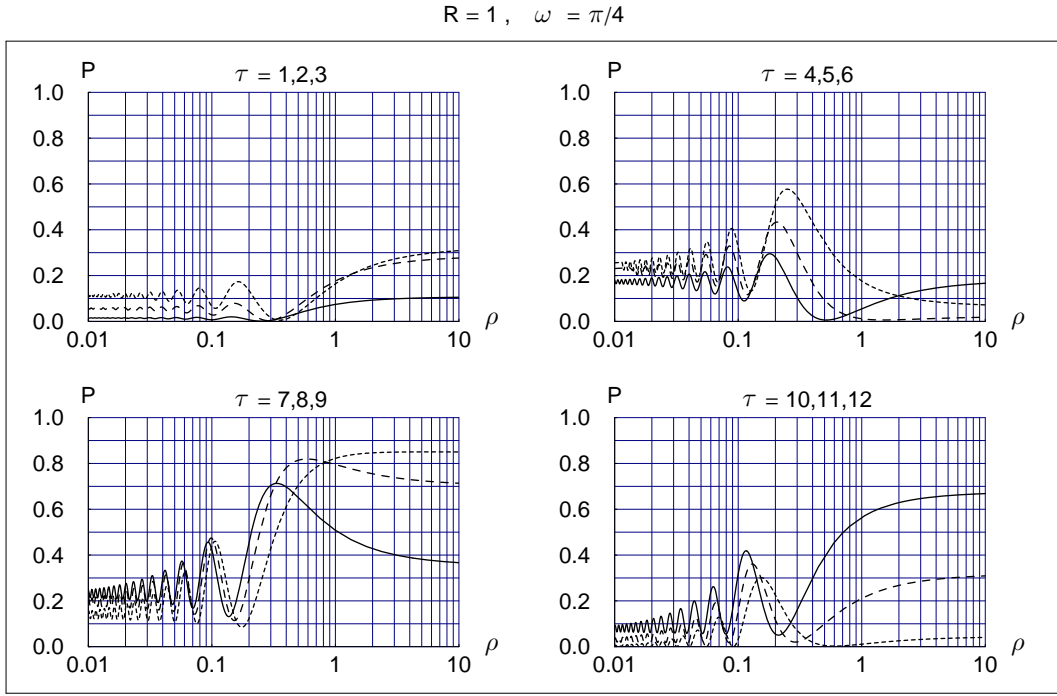


FIG. 5: Same as Fig. 4 but now for the generalized model with complex phase $\omega = \pi/4$.

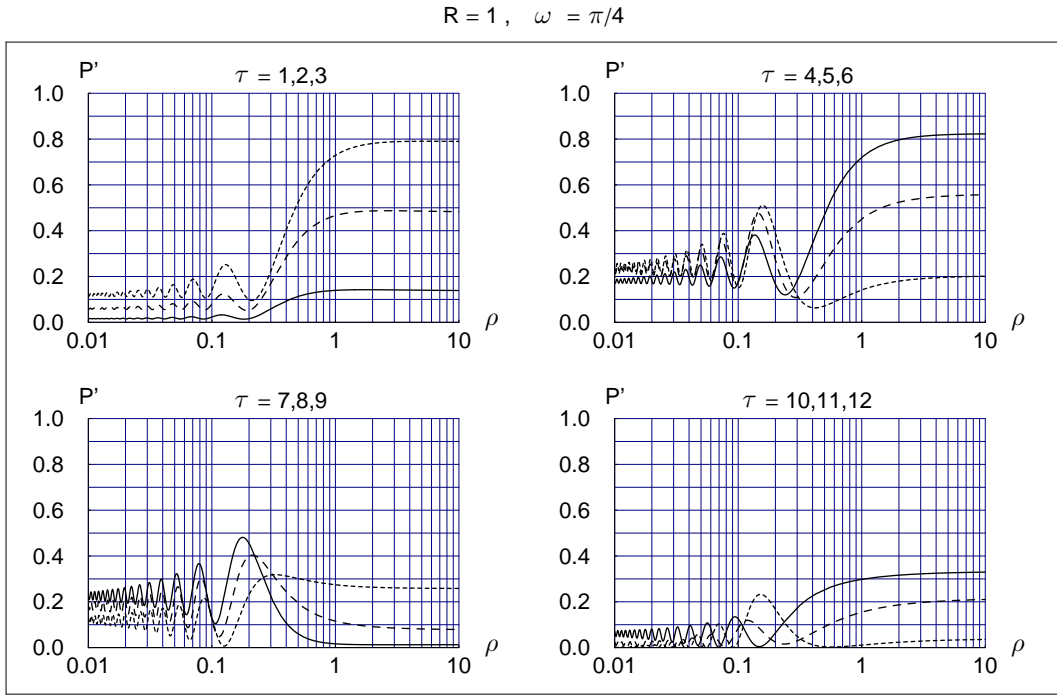


FIG. 6: Same as Fig. 5 but for the time-reversed process, with probability $P' \equiv P(\nu_e \rightarrow \nu_\mu)$. If CPT invariance holds, P' also corresponds to $P(\bar{\nu}_\mu \rightarrow \bar{\nu}_e)$.

$$\{R_m, \sin^2(2\theta_{13}), \delta; R, \sin^2(2\chi_{13}), \omega\} = \{1/30, 1/10, 0; 1, 1, \pi/4\}$$

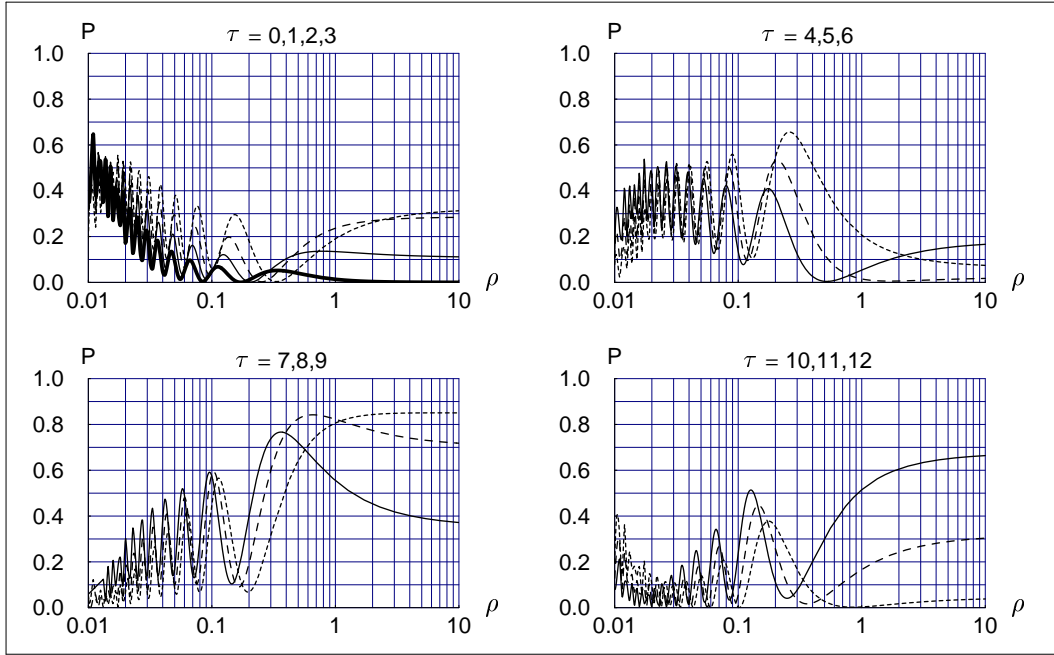


FIG. 7: Same as Fig. 5 but now for mass-sector parameters $R_m \equiv \Delta m_{21}^2/\Delta m_{32}^2 = 1/30$, $\sin^2(2\theta_{13}) = 1/10$, and $\delta = 0$. The heavy solid curve in the upper left panel has $\tau = 0$, corresponding to pure mass-difference neutrino oscillations.

$$\{R_m, \sin^2(2\theta_{13}), \delta; R, \sin^2(2\chi_{13}), \omega\} = \{1/30, 1/10, 0; 1, 1, \pi/4\}$$

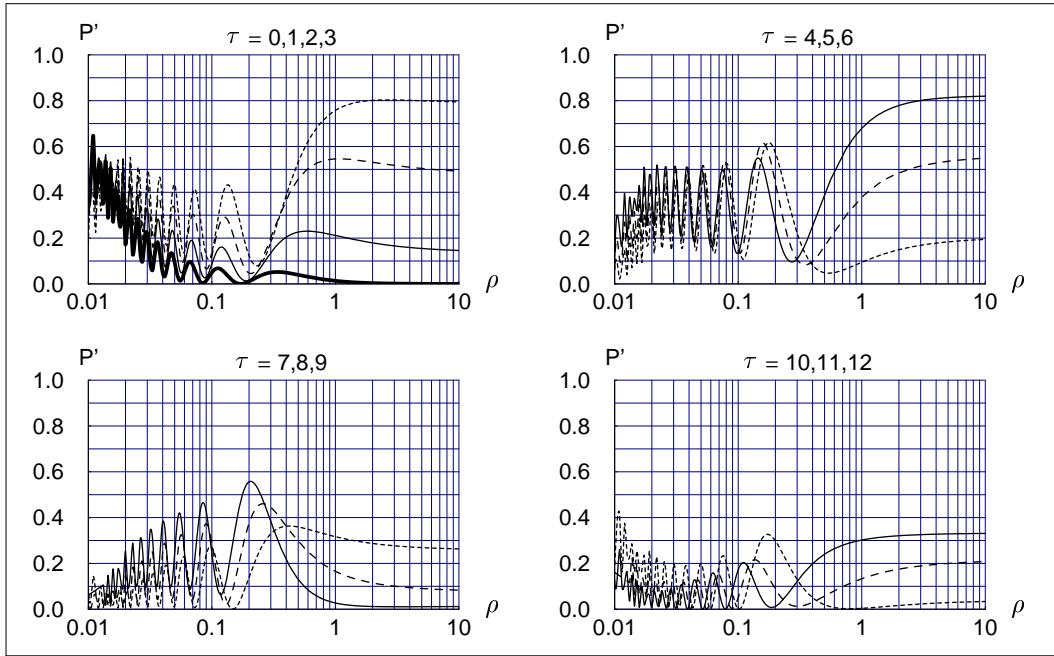


FIG. 8: Same as Fig. 7 but for the time-reversed process, with probability $P' \equiv P(\nu_e \rightarrow \nu_\mu)$. If CPT invariance holds, P' also corresponds to $P(\bar{\nu}_\mu \rightarrow \bar{\nu}_e)$.

$$\{R_m, \sin^2(2\theta_{13}), \delta; R, \sin^2(2\chi_{13}), \omega\} = \{1/30, 1/10, \pi/2; 1, 1, \pi/4\}$$

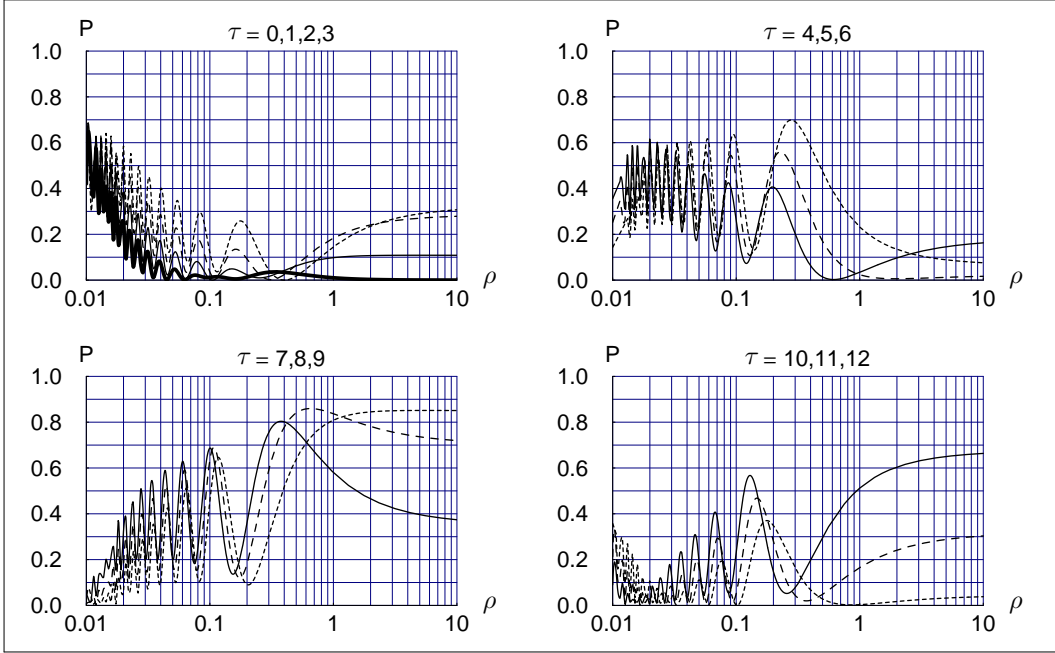


FIG. 9: Same as Fig. 7 but now for $\delta = \pi/2$.

$$\{R_m, \sin^2(2\theta_{13}), \delta; R, \sin^2(2\chi_{13}), \omega\} = \{1/30, 1/10, \pi/2; 1, 1, \pi/4\}$$

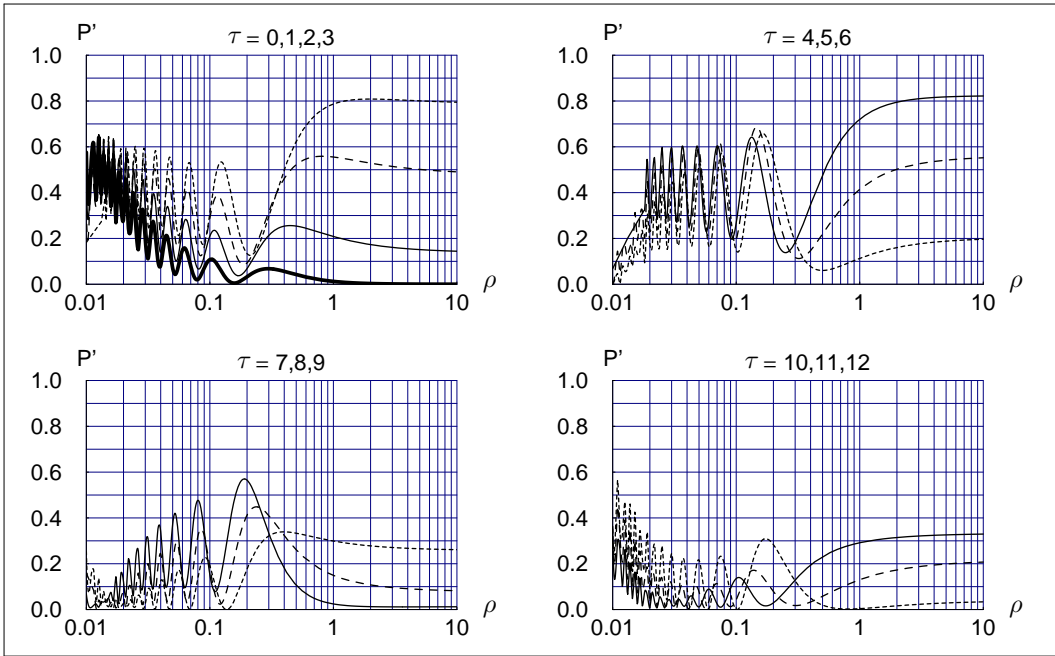


FIG. 10: Same as Fig. 9 but for the time-reversed process, with probability $P' \equiv P(\nu_e \rightarrow \nu_\mu)$. If CPT invariance holds, P' also corresponds to $P(\bar{\nu}_\mu \rightarrow \bar{\nu}_e)$.